Relationships between Acoustical Properties and Stiffness of Soft Tissue Phantoms

Barbara GAMBIN, Eleonora KRUGLENKO, Michał BYRA

Institute of Fundamental Technological Research, Polish Academy of Science,
Pawińskiego 5B, 02-106 Warsaw, Poland
bgambin@ippt.pan.pl, ekrug@ippt.pan.pl

Polyvinyl-alcohol cryogel is commonly used for soft tissue phantom manufacture. The gel formation from an aqueous solution of polyvinyl-alcohol takes place during the freezing and thawing cycle. The aim of this work was to assess the degree of gel solidification, hence the material stiffness, by means of quantitative ultrasound. We manufactured three phantoms which differed in the number of freezing/thawing cycles. First, tissue phantoms were examined with an elastography technique. Next, we measured the speed of sound and the attenuation coefficient. What is more, the inter structure variations in phantoms were assessed with the Nakagami imaging which quantifies the scattering properties of the backscattered ultrasound echo. Obtained results confirmed the connection between the number of freezing/thawing cycles and the solidification process. We defined the boundary layer as a region which has a different structure than the sample interior. Next, for each phantom this layer was extracted based on a Nakagami parameter map. We calculated that the thickness of the boundary layer was lower in samples which were subjected to a larger number of freezing/thawing cycles.

Keywords: soft tissue phantoms, elastography, ultrasound attenuation, speed of sound, Nakagami maps, stiffness.

1. Introduction

Poly(vinyl alcohol) (PVA) is a non-toxic industrial compound widely used, for example, in food packing. An aqueous solution of high-grade PVA is gelled into a cross-linked hydrogel by the formation of crystallites during repeated freeze/thaw cycles. After the freezing/thawing process, the obtained material is called PVA cryogel (PVA-c). The number of freeze/thaw cycles, the freeze time, the thaw time and the concentration of PVA in the aqueous solution, influence the number of crystallites formed and, as a result, the elasticity and several other properties of PVA-c [1]. PVA-c is commonly used as a soft tissue-mimicking material, suitable for medical

imaging studies. It has been used as a medical imaging phantom material in magnetic resonance imaging (MRI) from 1986, [2]. Additionally, it is used as tissue phantom in ultrasound imaging studies, because the acoustical properties of PVA-c materials are similar to those of soft tissues' acoustical properties like vessel tissue, breast tissue or liver tissue. The material is used as lesions tissue phantoms injected into tissue samples *in vitro* by physicians who are trained in biopsy technique, cf. [3]. Besides, PVA-c materials possess thermal properties similar to tissues, and are used to evaluate thermography measurements in breast tissue lesion' diagnosis, and to prove the possibility of visualization of thermal fields by ultrasound parametric imaging, see [4–7]. The materials have been used to evaluate ultrasound measurements of vessels [8]. The aim of our consideration consists in confirmation of the usefulness of ultrasound measurements as markers of variations in the elastic properties of samples; hence indirectly to connect ultrasound parameters with the structural changes, cf. [9]. Besides our interest in PVA-c material as soft tissue acoustical phantoms, it is well-known that the ultrasound stiffness measurement is a non-destructive and inexpensive technique. In materials with elastic moduli of the order of several kPa, classical, mechanical measurements are complicated and expensive. To confirm the increase of the sample stiffness with the number of freezing/thawing cycles, the elastography maps were obtained with a quasi-static strain imaging technique. Next, the speed of sound variations, and frequency dependent attenuation have been analyzed. Additionally, the scattering structures have been differentiated by means of Nakagami m-parameter maps calculated from the backscattered echo amplitudes. The idea of taking into account the scattering characteristics included in backscattered RF signal variations, to define the elastic properties of the soft tissue mimicking material has been formulated in [10]. The authors analyzed the influence of variations in elasticity by the Nakagami maps directly correlated with scatterers random distribution in space and variations in their reflectivities. They used the agar-gel materials with glass scatterers; hence, they controlled the different matrix properties and different density of scatterers. It has been shown how the Nakagami m-parameter can be used to distinguish different elastic properties of sample materials. Here, we explore the same idea of using the Nakagami maps to find characteristic markers in maps related to the increasing stiffness of three different PVA-c samples. Let us notice that the PVA-c microstructure is not similar to the simple matrix-inclusion structure considered in [10]. The multilevel, multiphase microstructure of PVA-c is rather like complicated porous material structure. The paper is organized as follows. In Section 2, a brief description of performed experiments, and obtained results, is presented. The structural properties of phantoms measured by Nakagami maps, and different characters of maps in defined regions of samples, are discussed in Section 3. In Section 4 the final remarks are given.

2. Materials and methods

2.1. PVA-c samples fabrication

A 10% by weight PVA in water solution had been used by us to form different PVA-c samples, obtained through subsequent freeze–thaw cycles. The samples were made by a solidification through the 24 hour freeze-thaw process in which temperature -20^{o}C was fixed for 12 h and 25^{o}C for the next 12 h. At first, the water solution of PVA at a temperature of 90^{o}C was prepared. Three types of tissue samples have been produced from the same PVA-c material, sample PVA-1, sample PVA-2 and sample PVA-3, they differ in the number of freeze-thaw processes: one, two and three cycles of 24 hours duration, respectively. Each of the samples had a cylindrical shape with height 50 mm and diameter 84 mm. PVA-c complex, multi-level

microstructure, with the different sizes of inhomogeneities is visible in Fig. 1.

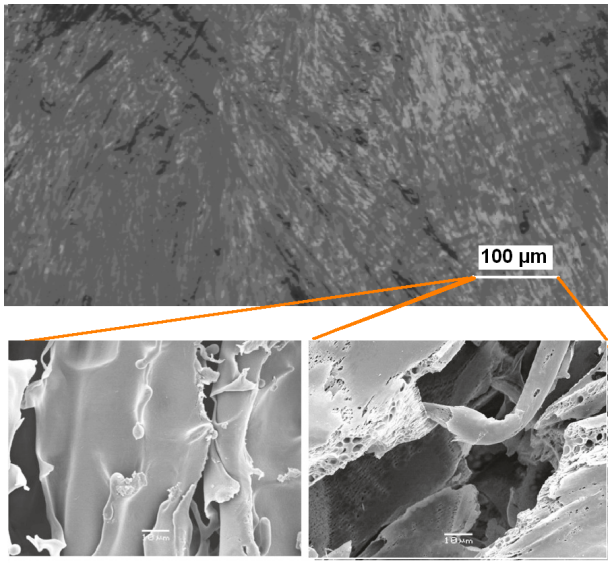

Fig. 1. Microstructure of PVA-c. Material microstructure, pictures size 600 x 900 mkm; optical microscope (Nikon Microphot) image with the lens Nikon BD plan 5x/0.1, pictures made by Dr. W. Secomski available by courtesy.

The microstructure presented in the two bottom figures of Fig. 1, has the inhomogeneities sizes very small with comparison to the typical ultrasound wave length used in the experiments. The typical wavelength was c/a 250 μm, so the subresolution scatterers could be only the oriented thin walls depicted in the top part of Fig. 1. The texture of the image is similar to the big grain of crystalline structure. This microstructure is non visible in USG B-mode images of all tree samples, called PVA-1, -2 and -3, see Fig. 2. In the B-mode images we can notice only the macroscopic inhomogeneities, looking like clouds.

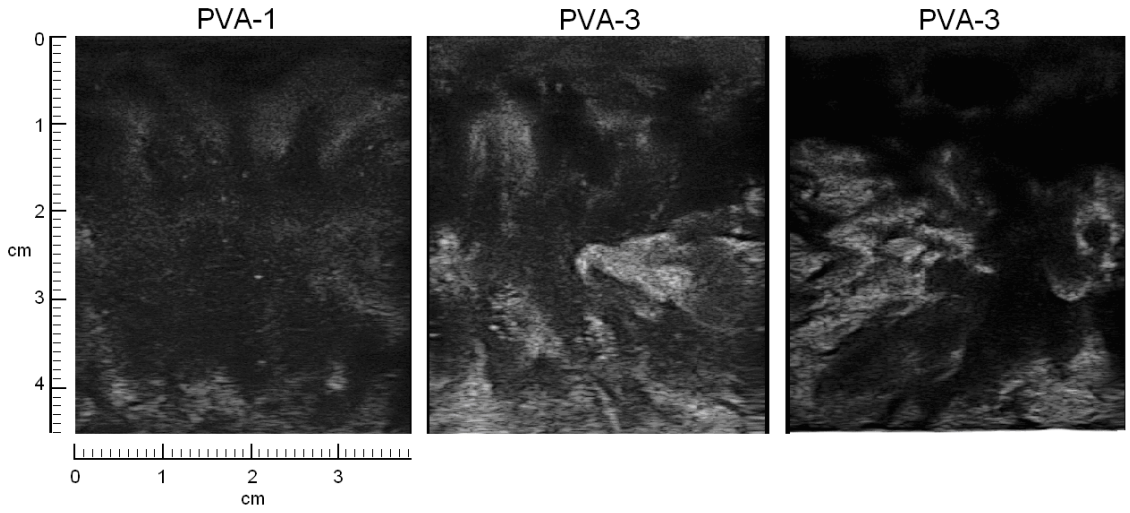

Fig. 2. B-mode different phantoms PVA-c.

2.2. Quantative differentiation of phantom stiffness

Samples with a greater number of cycles were harder, which could be noticed by squeezing the samples by hand. To compare sample stiffness, the pioneering ultrasound elastographic technique, quasistatic elastography, was applied with the use of the ultrasound imaging system ULTRASONIX SonixTouch (Analogic Corporation, Peabody, MA, USA), under the frequency of 13.3 MHz. Three images of simultaneously deformed two samples together were obtained, see Fig. 3. In this technique, an external compression is applied by hand to the sample, and the ultrasound images before and after the compression are compared. The areas of the image that are least deformed are the ones that are the stiffest, while the most deformed areas are the least stiff. An image of the relative distortions (strains) demonstrates a qualitative difference between the softer material in the sample on the left, and harder material on the right, respectively for each pair.

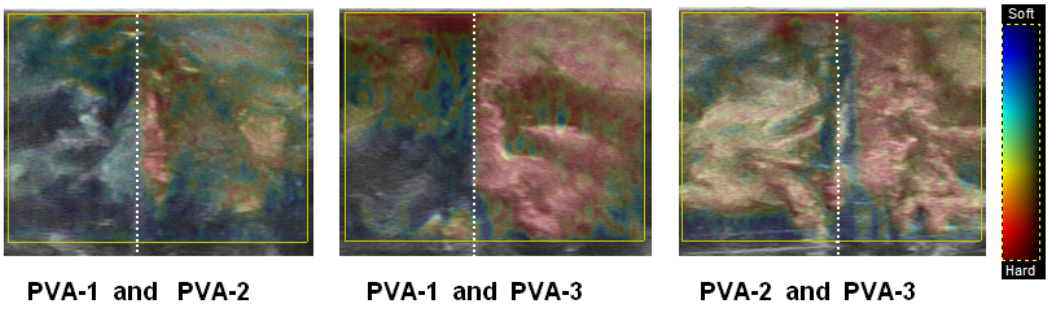

Fig. 3. Stiffness images. Comparison of two sample pairs.

2.3. Attenuation and speed of sound measurements

25 lines of RF signal were used to determine the attenuation coefficient, and speed of sound. Then, the results were averaged. The measuring system used to determine the acoustic characteristics consisted of the generator of pulses and receiver - Pulser/Receiver DPR 300, 6 MHz one element focusing transducer (Vermont) with focal length 62 mm, and diameter of 10 mm, RF signals were recorded with an oscilloscope - Agilent Technologies, DS09104A. For the attenuation and speed measurement, the focus was placed on the surface of the reflector lying on the bottom of the water container, see Fig. 4.

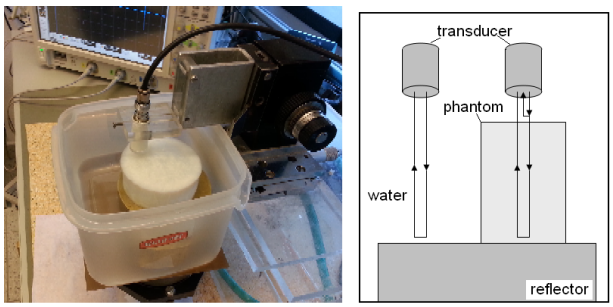

Fig. 4. Photo of experiment on the left side, scheme of the experiment right side.

Attenuation of ultrasonic waves was measured with the echo method on the basis of a comparison of pulses frequency spectra. First, a single pulse was sent in the water, and RF signals

reflected from the reflector were recorded. Next, the sample was placed in the water on the path of pulse propagation, and the procedure was repeated. Attenuation coefficient, depending on the frequency, was calculated using the formula (1):

$$\alpha(f) = \frac{-1}{2d} 20 \log_{10} \frac{|B(f)|}{|A(f)|} \tag{1}$$

where d - thickness of the sample, $|A(f)|$ and $|B(f)|$ - spectrum of reflected signal without phantom and with phantom, respectively. The attenuation coefficient frequency dependence is written in the form $\alpha(f) = \alpha_0 \cdot f$. The scheme of determination of the attenuation coefficient by the reflection method is depicted in Fig. 5. The attenuation coefficient is calculated by linear and quadratic regression, see Fig. 6.

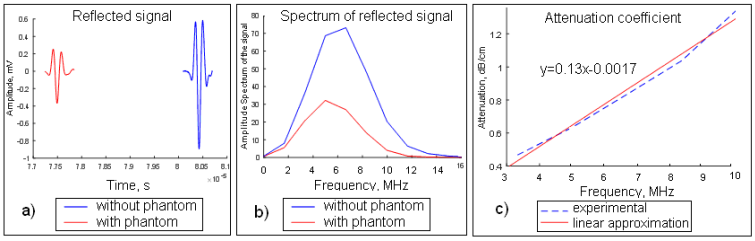

Fig. 5. The scheme of the attenuation coefficient determining.

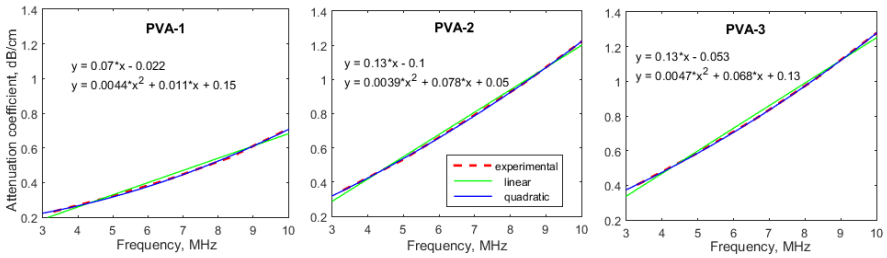

Fig. 6. The attenuation coefficient vs frequency, the experimental, its linear and quadratic regression lines.

Note that the attenuation coefficient for the soft tissue is c/a 0.6 dB/(cm·MHz), for water - 0.0022 dB/(cm·MHz) and for blood - 0.2 dB/(cm·MHz).

The speed of sound was calculated using the simple relation $c = 2d/\Delta t$, where d - the thickness of the phantom, Δt - time designated from the RF signal as the difference between the two reflections: the boundary water/phantom (the top) and the phantom/reflector (the bottom). The scattering from samples is very weak; hence, to determine the boundary of water/phantom (the distance from the transducer to the sample has been approximately 10 mm), a small metal wire was placed on that boundary, see Fig. 7. Values of attenuation coefficients, and speed of sound, for three different sample calculations are summarized in Tab. 1.

3. Statistics of RF backscattered signal

To study the statistics of the backscattered signal firstly, the signals were subjected to band-pass filtering around the transmit frequency, and compensation of attenuation was performed. Then the random amplitude data had been fitted to different probability distributions, which are

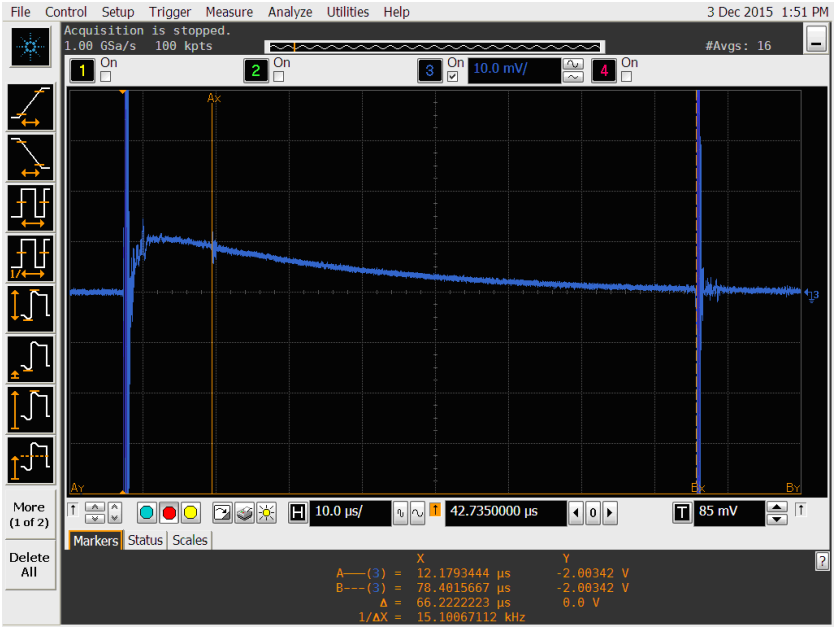

Fig. 7. Determining the time course of the pulse by sample, for the example in PVA-1 - 66.22 μs.

Tab. 1. Physical characteristics of different types of samples.

Sample	Number of cycles	Attenuation coefficient in dB/(cm·MHz)	Speed of sound in m/s
PVA-1	1	0.085 $\pm$ 0.009	1492$\pm$ 16
PVA-2	2	0.115 $\pm$ 0.015	1554 $\pm$ 28
PVA-3	3	0.124 $\pm$ 0.013	1559$\pm$ 31

commonly used to describe the nature of the scattering from soft tissues, cf. [7], particularly the Rayleigh distribution, Gamma, Rician and Nakagami and K-distribution. The Nakagami distributions were indicated as the closest to the data. Quantitative ultrasound imaging based on backscattered statistics serves as a complement to the ultrasonic B-scan technique, and can be used to evaluate the type of scatterers distribution and their concentration. RF signals were collected with the ultrasound scanner (Ultrasonix SonixTOUCH, British Columbia, Canada) equipped with the linear transducer L14-5/38. The center frequency and focus were set to 10 MHz and 3 cm, respectively. The pulse had 2 sinusoids, and its duration was 0.25 μs. The scanning volumes had dimensions 38 x 45 mm, the sampling infrequence 40 MHz, so 256 RF lines were obtained with 2336 points (data forms matrix of 2336 x 256 dimension). Volume of 1 x 1 mm contains 52 sampling points and 14 lines. Maps of the shape parameter of the Nakagami distribution of RF signals envelopes were calculated using a moving window technique with the window size of 2 x 2 mm [11]. At first, were calculated SNR (signal-to-noise ratio) maps, see Fig. 8.

$$\mathrm{SNR} = \frac{\mu}{\sigma}, \tag{2}$$

where μ is the signal mean or expected value, and σ is the standard deviation of the noise, or an estimate thereof. SNR values were in the range of 0.35-7.02; 0.32-6.82 and 0.28-5.85 for PVA-1, 2 and 3 respectively, see Fig. 8.

Let us remind ourselves, that the Nakagami distribution for the analytic signal envelope is

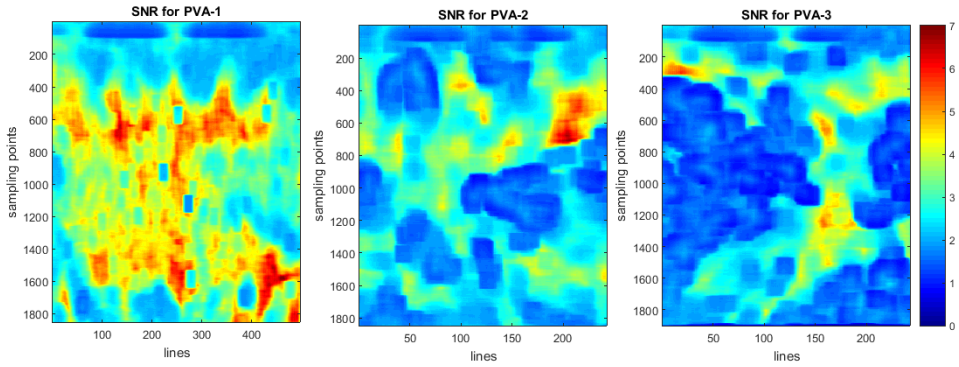

Fig. 8. SNR map for different phantoms.

statistically equivalent to the assumption of the Gamma distribution for the signal power. Indeed, the Nakagami shape m-parameter corresponds to the SNR for $[A^2]$, where A is amplitude of signal RF, and can be approximated as follows:

$$\mathrm{m} = \frac{\mathrm{E}^2[A^2]}{\mathrm{Var}[A^2]}, \tag{3}$$

where E is expected value and Var is variance.

It is well-known that for $\mathrm{m} = 1$ we have Rayleigh statistics of scatterers, $\mathrm{m} < 1$ corresponds to pre-Rayleigh statistics, i.e. less scatterers in the resolution cell, or stronger variability of scatterers' reflectivities. And, for $\mathrm{m} > 1$, a coherent signal from specular reflection is expected, in addition to the Rayleigh diffusive scattering.

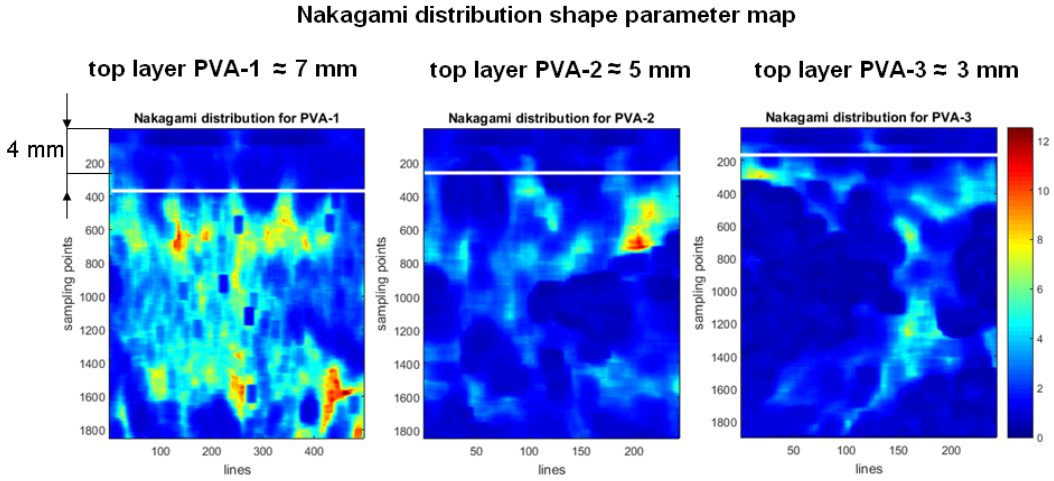

Fig. 9. Nakagami distribution shape parameter map for three different phantoms.

In the paper, the shape parameter Nakagami distribution m has been calculated using Matlab MLE - Maximum likelihood estimates. Parameter m values varied in the range of 0.14 - 12.45; 0.13-11.73; 0.12-8.57 for PVA-1, 2 and 3, respectively. The mean values of the parameter m in the entire area of PVA-1, 2 and 3 are 3.02, 1.69 and 1.35, respectively.

On the Nakagami maps, Fig. 9, the differences in samples are visible - larger areas with higher values of m-parameter are in the sample PVA-1. Map patterns of PVA-2 and PVA-3

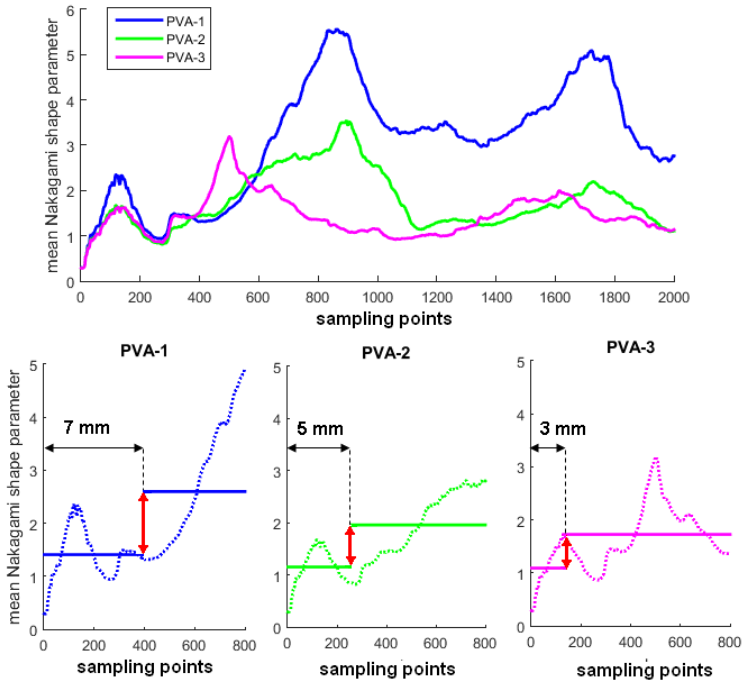

Fig. 10. Mean shape parameter Nakagami distribution.

have similar coloring, but we can distinguishe the different color of the top area. This fact can attest to the diversity of the material within the same pattern. To specify a boundary layer in each sample, the average value of the parameter m at different depths was calculated. Fig. 10 (top) shows plots of the average value of the parameter m, calculated from points on the same level of depth. Notice, that the value of m varies with depth in a similar way in each sample. To accurately determine the boundary layer thickness, we selected a point where the average value of the parameter m (in Fig. 10 - level line) increases almost twice. The jump between the mean values of the parameter m Fig. 10 (down) is shown by the red arrow. Boundary layer decreases, which is linked to the homogenization of the structure of the sample material with a greater number of freeze / thaw cycles. The areas from which the SNR in Fig. 8 and m-Nakagami in Fig. 9 have been calculated are denoted in Fig.11. Dependence of values of SNR and m-Nakagami distribution shape parameter for all the samples, from the area of the individual layers and the entire areas, are shown in Fig. 12.

4. Conclusion

The elastography measurements, see Fig. 3, confirm qualitatively the hierarchy of stiffness, namely the PVA-2 is stiffer than PVA-1, PVA-2 is softer than PVA-3 and the greatest difference in stiffness is between PVA-1 and PVA-3, as expected. Let us underline that the attenuation coefficients calculated by us are in agreement with the paper [2]. In that paper, the attenuation coefficients were in the range of 0.075–0.28 dB/(cm·MHz) for PVA-c phantoms, but the PVA-c material in this experiments had been prepared from a 20% PVA water solution, whereas we had used a 10% solution of the polymer. Speed of sound also increases with the number of cycles of freezing, and takes values 1492, 1554, 1559 m/s, respectively. It is greater than the speed of sound in water - 1490 m/s, and lower than the speed of sound in soft tissue 1540 m/s. In the study [2], the speed of sound of PVA-c phantoms was in the range from 1520 to 1540 m/s, but the

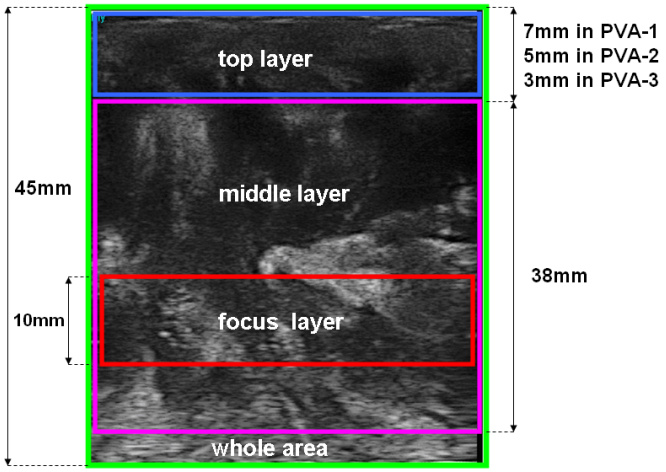

Fig. 11. Scheme of distribution of areas.

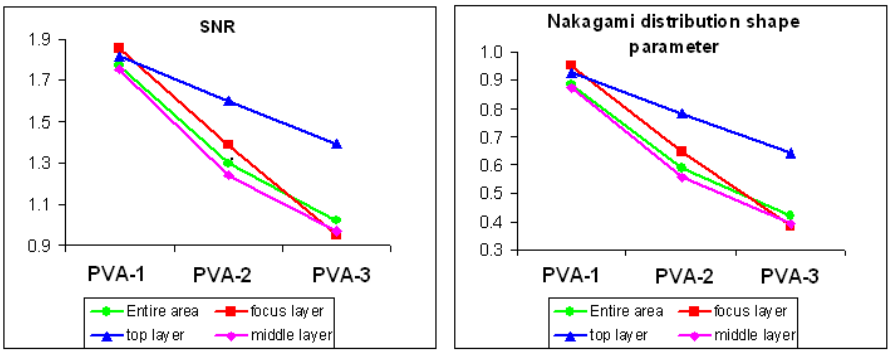

Fig. 12. Values of parameters for 3 phantoms and different areas.

PVA-c material contains a double amount of PVA. Table 1 summarized results of attenuation, and speed of sound, values. The values of densities of the samples ranged from 1047 kg/m^3 to 1231 kg/m^3. The PVA-c materials exhibit weak absorption, the attenuation coefficient has a small value, but its frequency dependence confirms the water like absorption for PVA-1 sample. After the next cycle of freezing/thawing the absorption frequency dependence starts to be closer to the tissue absorption. It can be measured by the distance from linear and quadratic regression lines. The PVA-1 has close to quadratic frequency dependence, while PVA-2 and PVA-3 have this dependence closer to linear dependency, like in tissue. The speed of sound increases with the sample numeration. Because the density of samples changes some order of magnitude less than stiffness variations, we can deduce that the speed of sound is the direct measure of stiffness in PVA-c materials. Additionally, comparing the Nakagami maps of the three samples, we notice the increasing values of m-Nakagami, together with increasing stiffness. Hence, divided areas of samples into subareas, boundary layers and internal regions can be extracted as areas with different substructures. As a result it has been demonstrated that boundary layers' thickness decreased with sample numeration, which is in agreement with the physical process of increasing samples' stiffness with subsequent freezing-thawing processes. We claim that the thicknesses of the boundary layers in stiffer samples indicate the direct connection of the local gelation process formation with the local stiffness distribution. Taking all results into account

we are able to conclude that acoustic characteristics differentiate the structure of PVA-c; by the frequency dependence of attenuation, values of speed of sound, and statistics of scattering structure illustrated by the Nakagami maps. A greater number of experiments is needed to estimate the accuracy of our acoustic markers of stiffness in PVA-c materials. Additionally, in the future an automatic segmentation of parametric maps can be used to extract the boundary layer [12].

ACKNOWLEDGMENT
This work was partially supported by the National Science Centre (2011/03/B/ST7/03347).

References

[1] J.L. Valentın, D. Lopez, R. Hernandez, C. Mijangos, and K. Saalwachter, Structure of Poly(vinyl alcohol) Cryo-Hydrogels as Studied by Proton Low-Field NMR Spectroscopy, Macromolecules, Vol.42, 263-272, 2009.

[2] K.J.M. Surry, H.J.B. Austin, A. Fenster and T.M. Peters, Poly(vinyl alcohol) cryogel phantoms for use in ultrasound and MR imaging, Physics in Medicine and Biology, Vol. 49, Number 24,5529-5546, 2004.

[3] W. Xia, D. Piras, M. Heijblom, W. Steenbergen, T.G. van Leeuwen, Srirang Manohar, Poly(vinyl alcohol) gels as photoacoustic breast phantoms revisited, Journal of Biomedical Optics, Vol. 16, no.7, 075002, 2011. doi:10.1117/1.3597616.

[4] B. Gambin, E. Kruglenko, Temperature Measurement by Statistical Parameters of Ultrasound Signal Backscattered from Tissue Samples, Acta Physica Polonica A, Vol. 128, 1-A, A-72 - A-78, 2015.

[5] M. Byra, B. Gambin, Temperature detection based on nonparametric statistics of ultrasound echoes, Hydroacoustics, Vol. 18, 17-23, 2015.

[6] E. Kruglenko, B. Gambin, RF signal amplitude statistics during temperature changes in tissue phantoms, Hydroacoustics, Vol. 17, 115-122, 2014.

[7] J. Mamou, M.L. Oelze, Eds., Quantitative Ultrasound in Soft Tissues, Springer 2013.

[8] Z. Trawiński, J. Wójcik, A. Nowicki, R. Olszewski, A. Balcerzak, E. Frankowska, A. Zegadło, P. Rydzyński, Strain examinations of the left ventricle phantom by ultrasound and multislices computed tomography imaging, Biocybernetics and Biomedical Engineering, Vol.35, 255-263, 2015.

[9] H. Mehrabian, A. Samani, Constrained hyperelastic parameters reconstruction of PVA (Polyvinyl Alcohol) phantom undergoing large deformation, Medical Imaging 2009: Visualization, Image-Guided Procedures, and Modeling, eds. M. I. Miga, K. H. Wong, Proc. of SPIE Vol. 7261, 72612G, 2009, doi: 10.1117/12.813871.

[10] P.-H. Tsui, Y.-L. Wan, Y.-T. Chien, C.-C. Yeh, C.-Y. Wang, Dependency of Ultrasonic Nakagami Images on The Mechanical Properties of Scattering Medium, Journal of Medical and Biological Engineering, Vol.33, 1, 95-102, 2013.

[11] M. Byra, A. Nowicki, H. Piotrzkowska-Wróblewska, J. Litniewski, K. Dobruch-Sobczak, Correcting the influence of tissue attenuation on Nakagami distribution shape parameter estimation, Ultrasonics Symposium (IUS), 2015 IEEE International, 1-4, 2015.

[12] M. Byra, A. Nowicki, H. Piotrzkowska-Wróblewska, K. Dobruch-Sobczak, Classification of breast lesions using segmented quantitative ultrasound maps of homodyned K distribution parameters, Medical Physics, Vol. 43, 5561-5569, 2016.